

Temporal properties of gamma ray bursts as signatures of jets from the central engine

F. Quilligan¹, B. McBreen¹, L. Hanlon¹, S. McBreen¹, K.J. Hurley¹, and D. Watson²

¹ Department of Experimental Physics, University College Dublin, Dublin 4, Ireland

² X-Ray Astronomy Group, Department of Physics and Astronomy, Leicester University, Leicester LE1 7RH, UK

Received / Accepted

Abstract. A comprehensive temporal analysis has been performed on the 319 brightest GRBs with $T_{90} > 2$ s from the BATSE current catalog. The GRBs were denoised using wavelets and subjected to an automatic pulse selection algorithm as an objective way of identifying pulses and quantifying the effects of neighbouring pulses. The number of statistically significant pulses selected from the sample was greater than 3000. The rise times, fall times, full-widths at half maximum (FWHM), pulse amplitudes and pulse areas were measured and the frequency distributions are presented here. All are consistent with lognormal distributions provided the pulses are well separated. The distribution of time intervals between pulses is not random but compatible with a lognormal distribution when allowance was made for the 64 ms time resolution and a small excess (5%) of long duration intervals that is often referred to as a Pareto-Lévy tail. The time intervals between pulses are most important because they may be an almost direct measure of the activity in the central engine. Lognormal distributions of time intervals also occur in pulsars and SGR sources and therefore provide indirect evidence that the time intervals between pulses in GRBs are also generated by rotation powered systems with super-strong magnetic fields. A range of correlations are presented on pulse and burst properties. The rise and fall times, FWHM and area of the pulses are highly correlated with each other. The pulse amplitudes are anticorrelated with the FWHM. The time intervals between pulses and pulse amplitudes of neighbouring pulses are correlated with each other. It was also found that the number of pulses, N , in GRBs is strongly correlated with the fluence and duration and that can explain the well known correlation between duration and fluence. The GRBs were sorted into three categories based on N i.e. $3 \leq N \leq 12$, $13 \leq N \leq 24$ and $N \geq 25$. The properties of pulses before and after the strongest pulse were compared for three categories of bursts. No major differences were found between the distributions of the pulse properties before and after the strongest pulse in the GRB. However there is a strong trend for pulses to have slower rise times and faster fall times in the first half of the burst and this pattern is strongest for category N . This analysis revealed that the GRBs with large numbers of pulses have narrower and faster pulses and also larger fluences, longer durations and higher hardness ratios than the GRBs with smaller numbers of pulses. These results may be explained by either homogeneous or inhomogeneous jet models of GRBs. The GRBs with larger number of pulses are closer to the axis if Γ varies with the opening angle of the jet and the imprint of the jet is preserved in the pulse structure of the burst. The distribution of the number of pulses per GRB broadly reflects the beaming by the jet.

Key words. Gamma rays – bursts: Gamma rays – observations: Methods – data analysis: Methods – statistical

1. Introduction

Much of the recent progress in the study of gamma-ray bursts (GRBs) results from the detection of bursts with good location accuracy by BeppoSAX that enabled the detection of counterparts at other wavelengths. The subsequent redshift determination of bursts have established that these bursts are at cosmological distances (Costa et al., 1997; van Paradijs et al., 1997). GRBs seem to be connected to massive stars and become powerful probes

of the star formation history of the universe (Lamb & Reichart, 2000; Hanlon et al., 2000; Berger et al., 2001). However not many redshifts are known and there is still much work to be done to determine the mechanisms that produce these enigmatic events.

The most plausible GRB progenitors are expected to be a newly formed black hole (BH) surrounded by a temporary accretion disk (Rees, 1999; Mészáros, 2001; Castro-Tirado, 2001). The most popular models include the merger of a neutron star (NS) and a NS (Eichler et al., 1989; Ruffert & Janka, 1999), NS and a BH (Paczynski,

1991), BH white dwarf merger (Fryer et al., 1999) and models of failed supernovae or collapsars (MacFadyen & Woosley, 1999; Paczynski, 1998). An important exception is the model in which the GRB energy is provided by a newly formed neutron star (Usov, 1992; Thompson, 1994). Various explanations have been put forward for the complicated structure of the light curves. These range from internal shocks, caused by variations in the velocity of the outflow (Rees & Mészáros, 1994; Piran, 1999), to external shocks, caused by interactions with an external medium (Mészáros & Rees, 1993; Dermer & Mitman, 1999). In the internal shock model the instabilities in the wind leads to shocks which convert a fraction of the bulk kinetic energy to internal energy remote from the central engine. A turbulent magnetic field then accelerates electrons which radiate by synchrotron emission and inverse Compton scattering, generating the GRB. Many of the observed features in bursts can be reproduced in the internal shock models of GRBs (Sari & Piran, 1997; Kobayashi et al., 1997; Daigne & Mochkovitch, 1998; Panaiteescu et al., 1999; Downes et al., 2001).

A variety of analytical techniques has been applied to the temporal and spectral profiles of GRBs which place constraints on the observed distributions which models must satisfy. The impressive results from these studies include (1) hard to soft evolution (Golenetskii et al., 1983; Borgonovo & Ryde, 2001); (2) the duration-hardness anticorrelation (Kouveliotou et al., 1993); (3) the temporal asymmetry of pulses in GRBs (Nemiroff et al., 1993; Link & Epstein, 1996); (4) a bimodal duration distribution of GRBs consistent with two lognormal distributions (Kouveliotou et al., 1993; McBreen et al., 1994); (5) the discovery of two different types of pulses in GRBs (Pendleton et al., 1997); (6) a correlation between E_{peak} and intensity (Mallozzi et al., 1995); (7) energy dependence of the pulse duration (Norris et al., 1996); (8) a relationship between the pulse peak energy, E_{peak} , and the photon fluence (Liang & Kargatis, 1996; Crider et al., 1999); (9) lognormal pulse shapes and time intervals between pulses in long (McBreen et al., 1994; Hurley et al., 1998) and short GRBs (McBreen et al., 2001); (10) spectra well fit with a Band function (Band et al., 1993); (11) spectral hardening before a count rate increase (Bhat et al., 1994); (12) an x-ray excess in GRB spectra (Strohmayer et al., 1998); (13) a correlation between complexity and brightness (Stern et al., 1999) and (14) the unique properties of the pulses and power law relationships between the pulse properties and durations of GRBs (McBreen et al., 2002).

While GRBs display hard to soft spectral evolution, there is remarkable constancy of the pulses in GRBs throughout the burst (Ramirez-Ruiz & Fenimore, 2000; Quilligan et al., 1999). The temporal and spectral properties of a few GRBs with known redshift have yielded two important results to suggest that GRB properties may be related to their luminosities. Ramirez-Ruiz and Fenimore (1999) have shown that more rapidly variable bursts have higher absolute luminosities. Norris et al. (2000) have

found an anticorrelation between the time delay in the arrival times of hard and soft photons in pulses and the luminosity of the GRB.

The light curves of GRBs are irregular and complex. Statistical studies are necessary to characterise their properties and hence to identify the physical properties of the emission mechanism. The statistical methods used for temporal studies can be broadly divided into four categories: (1) fits to individual pulses in the GRB using a number of pulse shape parameters (Norris et al., 1996; Lee et al., 2000b,a); (2) a non-parametric approach to pulse shapes in GRBs (McBreen et al., 1994; Hurley et al., 1998; Young et al., 1995; Quilligan et al., 1999); (3) the average statistical properties of GRBs using a peak-aligned profile (Stern & Svensson, 1996); and (4) the average power spectral density of GRBs (Belli, 1992; Beloborodov et al., 2000; Chang & Yi, 2000). One of the first studies (McBreen et al., 1994) revealed that lognormal distributions can adequately describe the properties of GRBs. Subsequent studies (Li & Fenimore, 1996; Hurley et al., 1998; Quilligan et al., 1999) have confirmed the applicability of lognormal distributions in accounting for the wide range in the observed properties of pulses in GRBs. This result is not surprising because lognormal distributions arise from the product of probabilities of a combination of independent events and such conditions apply to the pulse generation process in GRBs.

In a different approach (Beloborodov et al., 2000) used Fourier analysis to study the power spectral density of long GRBs. This approach revealed that the diversity of GRBs is due to random realisations of the same process which is self-similar over a range of time scales (Stern & Svensson, 1996). The slope of the PSD was $-5/3$ suggesting that GRBs are related to fully developed turbulence. The two different approaches are quite similar because the lognormal approach has been used to describe fully developed turbulence (Arneodo et al., 1999).

The work presented here expands on the earlier analysis (Quilligan et al., 2000) and provides new insight into the mechanism which generates GRBs. The aim is to provide a comprehensive description and understanding of the pulse properties in GRBs and combine it with other studies of the spectral properties. The wavelet analysis and the pulse selection algorithm are described in Sect. 2. The method for comparing the properties of the pulses before and after the strongest pulse in the GRB is also described in Sect. 2. The results are presented in Sect. 3, and discussed in Sect. 4. The conclusions are presented in Sect. 5.

2. Data Preparation

The dataset used was taken from the BATSE current catalogue. The ‘discsc’ files are available at <http://www.batse.msfc.nasa.gov/batse/grb/catalog/4b/> (Paciesas et al., 1999). The files contain the data from the four energy channels, which were combined into a single channel to maximise the signal to noise ratio. The

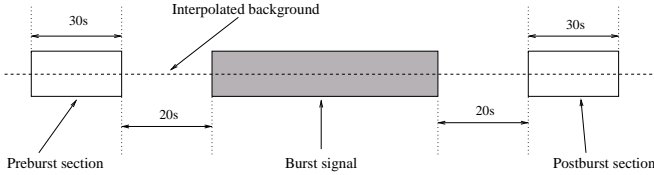


Fig. 1. Illustration of the background subtraction algorithm. The shaded region indicates the bursting phase of the GRB.

shapes of GRB pulses vary little with energy and pulses in different energy channels can be added together and nearly retain their initial shape. A subset of the BATSE catalogue was selected based on the criteria (Norris et al., 1996) that the GRB duration was greater than two seconds ($T_{90} > 2$ s) and the peak flux $P_{256\text{ms}} > 3.28$ photons $\text{cm}^{-2}\text{s}^{-1}$. In this way a sample of 324 bursts with good signal to noise and clearly resolved features was obtained. Five of these bursts could not be analysed properly due to data gaps, and so our final sample consisted of 319 GRBs. All 319 GRBs were used for the timing analyses. The 250 GRBs that were summed over only two LAD detectors were used for all analyses involving pulse amplitude and area.

2.1. Background subtraction

The first step in the data preparation involved selecting the appropriate background for subtraction from the GRB. The start and end times for each burst were identified. A further margin of 10 seconds was added to both the beginning and end of this chosen section. Two background sections of duration 30 s were then selected, one finishing 20 s before the start of the section containing the burst and the other starting 20 s after the end of the burst (Fig. 1). These two regions were used to fit a linear background that was subtracted from the burst section.

2.2. Denoising technique

One of the difficulties in analysing the time profiles of GRBs is in overcoming the limitations imposed by the presence of noise in the signal and the overlap of the individual pulses. The transient nature of GRBs also means that the usual assumptions for Fourier transform techniques do not hold (Chang & Yi, 2000; Suzuki et al., 2001). An alternative method of filtering the signal is with wavelets. Wavelet analysis was pioneered by Daubechies (1992) and others during the 1980's (Meyer, 1993).

Wavelets are specific functions that, when convolved with the signal under investigation, produce a transformed signal that represents the location and strength of variations within the original data. The convolution is applied repeatedly to the data over a range of scales with the convolution function gradually stretched to coarser and coarser scales, revealing variations at corresponding scales

in the original signal. This iteration with scaling of the convolved function allows the identification of structure with a variety of extents both in the spatial and frequency domains.

If the wavelet function is written as $\psi(x)$ then, more formally, the transform at a particular scale s , can be written as

$$W_s f(s, x) = f * \psi_s(x)$$

where $\psi_s(x) \equiv (1/s)\psi(x/s)$ represents the wavelet dilated by a scale factor s . At each scale 2^j , a discrete wavelet transform that we denote by $W_{2^j}^d$ can be computed. For the particular choice of scale, $s = 2^j, j = 1 \dots J$ the sequence

$$\left\{ S_{2^j}^d, (W_{2^j}^d f)_{1 \leq j \leq J} \right\}$$

is called the discrete dyadic wavelet transform of the input discrete signal $D = (S_1 f(n))_{n \in \mathbb{Z}}$. The $W_{2^j}^d f$ components provide the *detail* at each scale, meaning the response of the (scaled) wavelet function to the detailed variation of the signal. The coarse signal, $S_{2^j}^d$, provides the low frequency (slowly varying) component of the signal remaining at scales larger than 2^j . The higher frequency components can all be recovered from the dyadic wavelet transform $(W_{2^j}^d f)_{1 \leq j \leq J}$ between scales 2^1 and 2^J . A fast algorithm for calculating the wavelet transform of a signal was developed by Mallat & Zhong (1992) and implementation of this algorithm is at the core of the denoising procedure used. In Fig. 2, GRB 920513 is shown together with its dyadic wavelet transform for scales $s = 2^{2 \dots 4}$ (the lowest scale, $s = 2^1$, is not shown because it is dominated by noise). The transforms at each of the scales are shown (Fig. 2c, d and e), along with the low frequency signal $S_{2^4}^d$ containing the remaining information for scales $i > 4$ (Fig. 2f).

The function $\psi(x)$ used in the algorithm was chosen so that the wavelet acts like an edge detector with a delta response function to a step edge. In fact $W_{2^j}^d f$ is proportional to the derivative of the original signal smoothed at the scale 2^j . Thus calculating the positions of the modulus maxima of the transform, $|W_{2^j}^d f|$, is analogous to locating the sharp variations in the original signal. Mallat & Zhong (1992) also developed an algorithm for allowing the reconstruction of a signal given just the modulus maxima of the wavelet transforms across a set of scales along with the low frequency signal remaining at the coarsest scale. This reduced representation can reconstruct an accurate copy of the original, using an iterative algorithm that converges quite quickly to acceptable levels.

A technique for identifying white noise and removing it without losing any other information was introduced by Mallat & Hwang (1992). This technique relies on characterising the behaviour of noise across the various scales in the wavelet transform using just the information present in the extrema wavelet representation described in the previous paragraph. The change in the

amplitude of the extrema between scales allows the number called the Lipschitz exponent to be calculated. More precisely, each extremum describes a particular curve in $(\log(s), \log|Wf(s, x)|)$ space representing its increase or decay on all the scales for which $Wf(s, x)$ has been computed. Then the Lipschitz exponent, α , is just the maximum slope of a straight line that remains above this curve (Young et al., 1995). Using results from an analysis of white noise ($\alpha < -\frac{1}{2}$, Mallat & Hwang (1992)), as well as the investigation described below, the characteristic distribution of Lipschitz exponents for the noise present in BATSE GRB profiles was determined. In general, noise is expected to have a negative Lipschitz exponent indicating a decreasing amplitude with increasing scale. Extrema in the wavelet transform which fall in the range expected for noise can be removed using an algorithm developed for this purpose.

As an example consider the extremum at around 110 s on the top (finest) scale of GRB 920513 (Fig. 2c). On the next scale, the amplitude of this extremum is considerably smaller and by the following scale it is hardly detectable. It is clear that this extremum corresponds to a noise feature in the original signal and visual examination of the transform indicates that the amplitude of the wavelet transform decays quickly when moving to progressively coarser scales, as expected for noise. The extremum at around 95 s corresponds to a pulse with intensity over 25,000 counts per 64 ms. The amplitude of the wavelet maximum increases on coarser scales, contrary to the behaviour expected for noise.

The extrema removal algorithm was combined with a simple thresholding procedure based on the analysis of a section of the burst background. For each burst being prepared, a section of the same burst well separated from the signal was used to generate the wavelet transform of the background. The standard deviation of the transform at the scale 2^2 (the finest scale not dominated by noise) was combined with a significance level (σ_T) to calculate an amplitude threshold for the wavelet coefficients of the signal at the same scale. Any extrema in the signal with amplitudes less than this threshold on scale 2^2 were assumed to be due to noise and were removed.

A denoised signal was then reconstructed (e.g. Fig. 2a) using the algorithm described by Mallat & Zhong (1992). The reconstructed functions have no spurious oscillations or sharp variations, and are very similar to the original signal. The residuals between the background subtracted burst and the reconstructed burst are shown in Fig. 2b. The residuals were calculated assuming that the errors in the raw data were Poisson distributed. The variation of the residuals in the section containing signal do not differ significantly from a section due to background noise (Fig. 2b).

2.3. Pulse selection

Each pulse was examined to find minima on each side which were separated in amplitude from the maximum by more than a chosen significance level. If the search for minima failed on a pulse it was rejected and the search for pulses continued. The algorithm was designed so that the maximum and minima finally selected for a given pulse were the extreme values in that region of the signal. The significance level of the maxima and minima was calculated by multiplying the error on the counts by a scale factor, τ_σ . Given two data points n_1 and n_2 , where $n_1 > n_2$, the points overlap if

$$(n_1 - \tau_\sigma \Delta n_1) < (n_2 + \tau_\sigma \Delta n_2)$$

The errors on the counts in the cleaned signal were assumed to be Poissonian.

The pulse selection process is illustrated in Fig. 3. Starting with pulse 2, minima 1 and 3 were easily identified. Next, pulse 4 was considered. Pulse 4 overlaps the adjacent minimum 3 (based on appropriately sized error bars) and both turning points were rejected and minimum 5 was considered as the true minimum associated with pulse 2. A minimum, maximum, minimum triplet consisting of points 1, 2 and 5 was found. At the conclusion of the analysis the overlapping maxima/minima pairs consisting of points 6 and 7, 9 and 10 and 13 and 14 were rejected. The algorithm selected points 2, 8 and 12 as the maxima and identified associated minima 1, 5, 11 and 15.

The analysis was then extended to allow the identification of pulses that were well separated from their neighbours such that the overlap from the surrounding signal did not significantly affect the profile of the pulse. The fraction of the total height, H_b , (from pulse to background) which was above the higher minimum was determined and a threshold was applied to this fraction, above which pulses were considered isolated. In Fig. 3 the pulses 8 and 12 are not very well separated from their neighbours whereas pulse 2 is effectively isolated and not strongly influenced by surrounding signal. The fractional isolated height of pulse 8 (to which the threshold is applied) was obtained using (Fig. 3):

$$f_I = \min(H_l, H_r)/H_b = H_r/H_b = 8/21 \approx 0.38,$$

where H_l is the height difference between the pulse 8 and the point 5 on the left and H_r is the height difference between the pulse 8 and the point 11 on the right.

For pulse 2 (with point 1 being the higher minimum the smaller height difference is on the left) the estimate is:

$$f_I = \min(H_l, H_r) = H_l/H_b = 15/17 \approx 0.88.$$

Thus, if the threshold, τ_I , were set above $\sim 40\%$ then pulse 2 would be accepted as isolated and pulse 8 would be rejected. This method provided an objective way to identify and quantify pulses that were influenced by neighbouring signals.

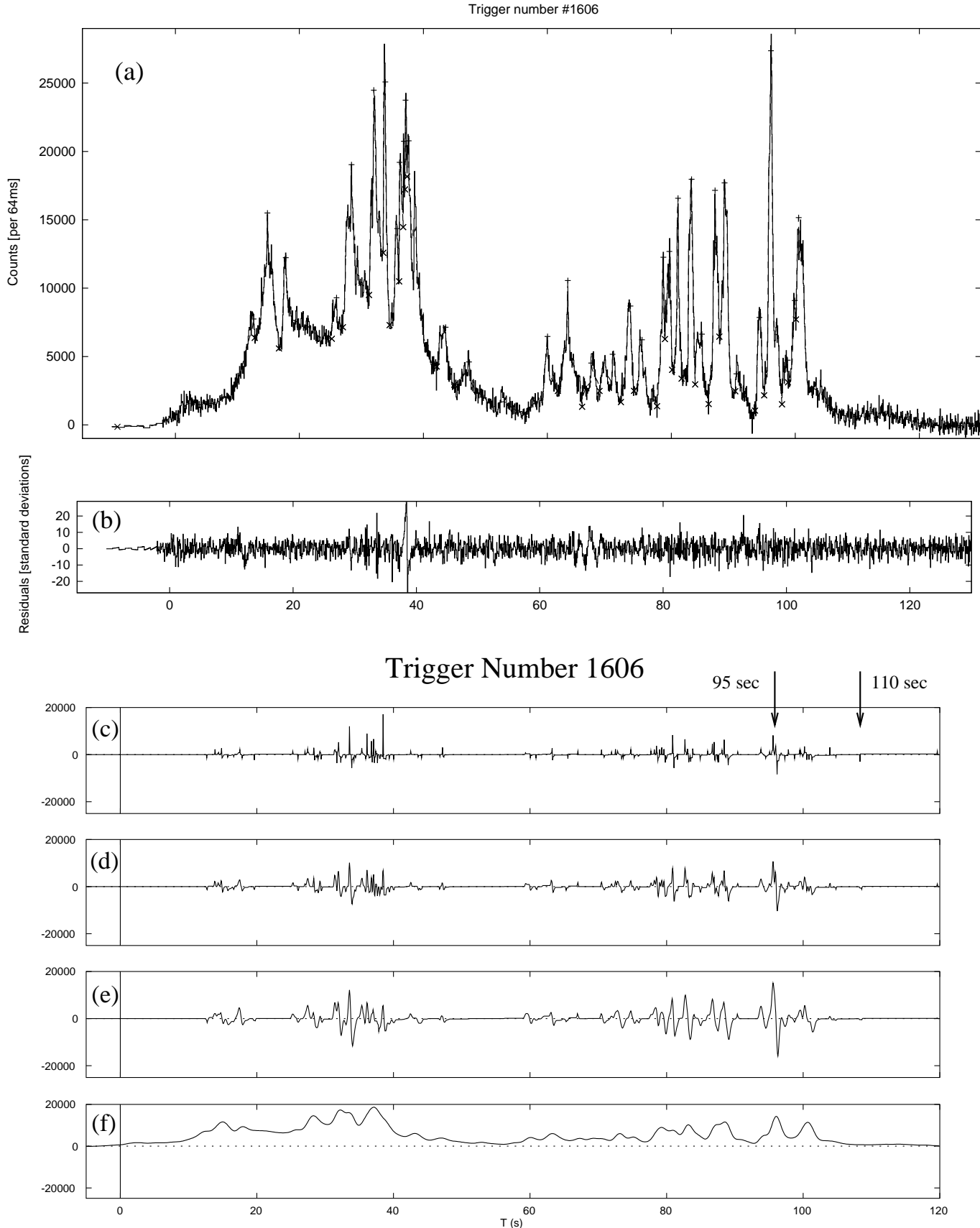


Fig. 2. The wavelet reconstruction of GRB 920513. (a) The GRB profile and wavelet fit with maxima (identified by the + symbol) and minima (identified by the x symbol). A total number of 33 pulses were identified above a threshold of 5σ . (b) The residuals between the wavelet fit and the actual GRB profile. (c)-(e) The decomposition of GRB 920513 (BATSE trigger 1606) into its component wavelet scales. The wavelet transform for scales $s = 2^{2\ldots 4}$ (the finest scale, $s = 2^1$, is not shown because it was dominated by noise). (f) The low frequency signal $S_{2^4}^d$ containing the remaining information for scales $i > 4$.

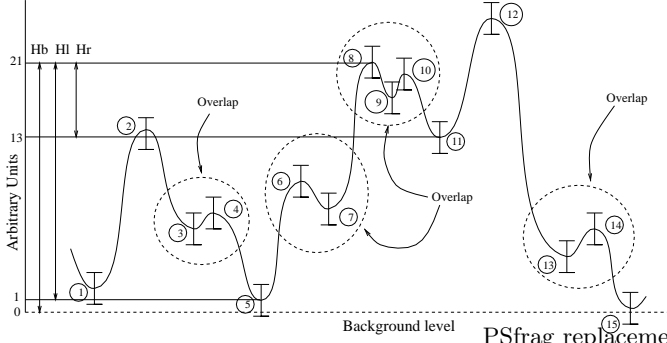


Fig. 3. A diagrammatic representation of the algorithm for identifying pulses with appropriate significance. The error bars were calculated using the count rate in the particular bin, multiplied by the threshold significance level, τ_σ . The dashed circles highlight maxima and minima where the error bars overlap. Larger values of τ_σ eliminate overlapping regions that were more widely separated. With a slightly smaller choice of τ_σ in this example, pulses 6 and 14 would have been accepted.

2.4. Properties of the pulses

The next task was to characterise the GRB profiles based on the properties of the constituent pulses. The following characteristics which had been studied previously (McBreen et al., 1994; Li & Fenimore, 1996; Hurley et al., 1998) were investigated: the number of pulses per burst, N ; the time intervals between pulses, ΔT ; the pulse amplitudes, C ; the pulse area, A_p ; the rise and fall times, t_r and t_f ; and the pulse durations or full width at half maximum, FWHM;

The total number of pulses in the sample of 319 GRBs was determined for a range of thresholds τ_σ and varying isolation levels, τ_I (Fig. 4). The variation in isolation level has a much larger effect on the sample than the threshold, and caused a reduction in the number of pulses from over 3000 at the isolation level of 20% to under 800 at the 80% level. Fig. 4 also shows that the number of pulses falls quite quickly as τ_σ increases from 3 to 5. The initial rapid reduction in the number of pulses selected may be an indication of the removal of the small population of noise pulses remaining after the denoising process. The total number of pulses is not very sensitive to the threshold level in the region of 5σ . The 319 GRBs are listed in Table 1, along with the total number of pulses above 5σ for each burst. Also included in the table are the number of isolated pulses at and above the 50% and 75% levels.

In the analysis of pulse shapes, non-parametric methods were used to estimate the various characteristics of the pulse profiles. This approach was chosen to make the conclusions more robust since no assumptions were made about the pulse shapes. Also since the measurements are made on the isolated pulses selected by the algorithm, the degree of isolation can be varied arbitrarily. If a particular measurement was sensitive to influence from surrounding pulses then the threshold τ_I was increased until the in-

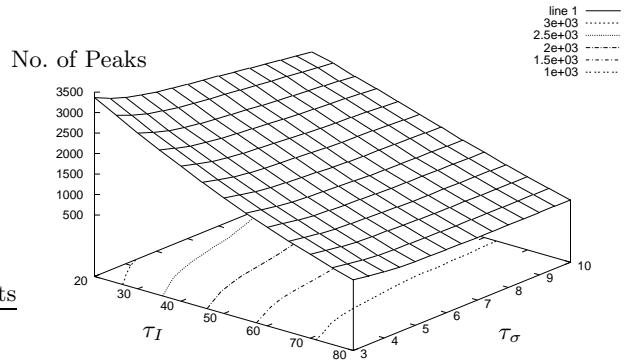


Fig. 4. The number of pulses selected from the 319 GRBs as a function of the isolation level τ_I and the threshold τ_σ . The plot also shows a projection of the data on to the τ_I, τ_σ plane and the contour levels are as given in the legend.

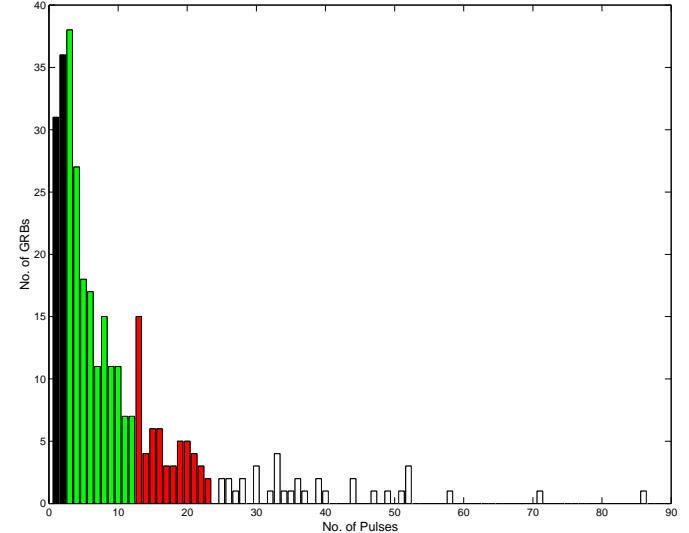


Fig. 5. The distribution of the number of pulses (N) per GRB. The shaded regions highlight the division into four categories, namely M, N, O and P with $1 \leq N \leq 2$, $3 \leq N \leq 12$, $13 \leq N \leq 24$ and $N \geq 25$ respectively.

fluence was reduced sufficiently, with the proviso that the number of pulses in the sample remains statistically useful.

The classification of pulses into isolated and non-isolated categories based on the algorithm allowed the measurement of characteristics of the temporal profile which are affected by neighbouring signals. The level of interference between pulses and the surrounding signal is dependent on the threshold at which the selection of these pulses is made. In fact a broad range of threshold levels were used to examine the time profiles and τ_I was typically varied from 20% to 80%. It was decided based on these results to adopt pulses with $\tau_\sigma \geq 5\sigma$ and $\tau_I \geq 50\%$ for the main analysis of the pulse properties.

The pulse amplitude was measured as the maximum count in a 64 ms time interval after background subtraction. The pulse area was measured using the sum of the background subtracted count rates starting at 5% of the height of the pulse above the left minimum to 5% of the pulse height above the right minimum on the falling edge of the profile. The starting point at 5% above the minimum was chosen to eliminate contributions from background noise for pulses with minima widely separated from the maximum.

For similar reasons the rise time was measured from 5% of the height of the pulse above the left minimum to 95% of that height. The upper value of 95% ensures that the finishing point is robust against flat topped pulses and noise in the profile near the maximum. The fall time was measured in a similar way to the rise times i.e. from 95% to 5% of the pulse height above the right minimum.

The duration of the individual pulses was measured using the FWHM of the pulse. This approximation is valid only for well isolated pulses and tended to give poorer estimates for the true pulse width as the effect of neighbouring signals increased and the left and right minima of the pulse rose out of the background.

2.5. Number of pulses per GRB

The frequency distribution of the number of pulses (N) per GRB is given in Fig. 5. N has a range from 1 to 86 with a peak at a value of 3, a median of 6 and only 10% of GRBs have $N \geq 25$. For convenience N is divided into four categories (Fig. 5). There are 34 GRBs in category P and only 7 have $N > 50$. Many of the timing studies on GRBs have concentrated on the categories with large N (e.g. Norris et al. 1996; Li & Fenimore 1996), which means that these analyses have focussed solely on the tail of the distribution shown in Fig. 5.

3. Results

3.1. The Lognormal distribution

It has been shown previously that the lognormal distribution can adequately describe the properties of GRBs (Quilligan et al., 1999). The lognormal distribution is generated by statistical processes whose results depend on a product of probabilities arising from a combination of events (Aitchison & Brown, 1957). A positive random variable X is said to be lognormally distributed if $Y = \log(X)$ is normally distributed with mean μ and variance σ^2 . The probability density function is:

$$f(x) = \begin{cases} \frac{1}{\sqrt{2\pi}\sigma x} \exp(-(\ln x - \mu)^2/2\sigma^2) & x > 0 \\ 0 & x \leq 0 \end{cases} \quad (1)$$

The median of the distribution occurs at $x = e^\mu$. Many examples of lognormal distributions occur in nature, such as the propagation of a laser beam in a turbulent medium,

the size of cumulus clouds in the atmosphere and terrestrial lightning (Uman, 1987; McBreen et al., 1994). In the case of terrestrial lightning, the durations, peak currents, intervals between the strokes in the flashes, and the flash charges are all lognormally distributed. The statistical properties of strokes in lightning discharges in the Earth's atmosphere have a close resemblance to the statistical properties of pulses in GRBs. In both cases the result depends on a multiplicative process arising from a combination of independent events.

3.2. Pulse analysis

3.2.1. FWHM of pulses

The distribution of the FWHM of the pulses from 319 GRBs and the best lognormal fit are given in Fig. 6a. Fig. 6b shows the same data plotted as a cumulative percent on logarithmic probability paper such that a lognormal distribution yields a straight line. All pulses have $\tau_\sigma \geq 5$ and $\tau_I \geq 50\%$. The distribution is very broad with a maximum at 0.7 s and half widths at 0.14 s and 3.5 s. The value of the reduced χ^2 is 0.3 showing the data is well fit by the lognormal distribution. In obtaining χ^2 , the part of the fit below 0.1 s was not included because of the distortion caused by the limited time resolution that is apparent in Fig. 6b. The value of the reduced χ^2 for the best lognormal fit as a function of τ_σ and τ_I are given in Figs. 6c and 6d. The fits are acceptable over most of the range with the largest departures occurring at the lowest values of τ_σ and τ_I because of the serious effects of pulse pile up. The lognormal distribution is a better fit when the effects of the overlapping pulses are reduced. The parameters of the best lognormal fit for $\tau_\sigma \geq 5$ and $\tau_I \geq 50\%$ are given in Table 2.

3.2.2. Rise time and fall times of the pulses

The distribution of the rise times of the pulses and the best lognormal fit are given in Fig. 7a. Fig. 7b shows the same data plotted as a cumulative percent and the large count in the first bin is due to the 64 ms resolution of BATSE. The parameters of the best lognormal fit to the broad distribution are listed in Table 2. The value of the reduced $\chi^2 = 1.3$ show the data is compatible with the lognormal distribution.

The distribution of the fall times of the pulses and the best lognormal fit are given in Fig. 8. The parameters of the best lognormal fit to the data are given in Table 2. The fall times are also compatible with the lognormal distribution and have a wider range with a slightly larger mean than the rise times.

3.2.3. Areas and amplitudes of the pulses

The distributions of the amplitudes and areas of the pulses with $\tau_\sigma \geq 5$ and $\tau_I \geq 50\%$ from 250 GRBs, summed over two detectors, and the best lognormal fits are given in Fig.

Table 1. The BATSE trigger number of the GRBs used in the analysis. N is the total number of pulses in the GRB, N(50/75) are the numbers of pulses that are isolated at and above the 50% and 75% levels respectively.

GRB	N	N(50/75)												
105	4	3/2	1974	2	0/0	2994	36	20/6	3929	3	2/1	6113	5	3/1
109	19	10/2	1997	13	8/2	3001	3	3/2	3930	19	6/1	6124	30	14/5
130	11	5/1	2037	6	5/3	3035	21	4/1	3936	5	1/1	6168	2	1/1
143	13	6/3	2053	1	1/1	3039	5	3/1	3954	1	1/1	6198	10	1/1
179	4	3/2	2067	8	1/1	3042	19	12/6	4039	33	21/7	6235	6	3/1
219	13	4/3	2080	26	12/2	3057	52	3/1	4048	9	3/3	6242	3	3/3
222	6	0/0	2083	2	2/1	3067	8	4/3	4312	4	2/1	6251	3	3/2
249	21	4/1	2090	15	7/2	3105	30	19/9	4368	12	2/2	6266	9	2/1
394	25	13/3	2110	13	3/1	3110	13	8/3	4556	3	1/1	6274	18	16/6
451	2	2/2	2138	6	2/2	3115	9	6/3	4701	20	8/4	6303	1	1/1
467	3	1/1	2151	3	3/3	3128	36	13/1	4814	2	1/1	6321	3	3/3
469	1	1/1	2156	39	8/3	3138	4	2/1	5080	7	7/3	6329	9	1/1
503	1	1/1	2213	5	5/2	3178	6	3/1	5304	14	0/0	6335	2	2/2
543	3	2/1	2228	28	12/5	3227	17	5/3	5389	13	7/3	6336	3	0/0
647	3	1/1	2232	14	8/6	3241	15	10/3	5417	2	0/0	6397	1	1/1
660	2	2/1	2316	1	1/1	3245	71	24/6	5419	2	1/1	6400	3	3/3
676	4	2/1	2321	11	4/1	3255	12	6/3	5439	4	4/3	6404	13	7/2
678	52	21/6	2329	20	3/1	3269	15	13/7	5447	2	1/1	6413	8	7/3
829	3	0/0	2362	2	2/2	3287	10	6/1	5450	13	5/4	6422	2	0/0
841	6	6/3	2367	3	3/2	3290	6	4/3	5451	2	0/0	6436	3	3/3
869	10	4/1	2371	2	2/1	3306	16	13/4	5470	7	4/4	6451	3	2/1
907	4	3/2	2387	1	1/1	3330	13	5/3	5473	39	27/19	6453	25	5/1
973	3	1/1	2393	2	1/1	3345	4	1/1	5477	12	9/5	6472	47	18/5
999	2	2/2	2431	1	1/1	3351	10	7/5	5486	12	1/1	6525	8	6/5
1025	4	2/1	2436	11	8/2	3408	44	17/5	5489	16	8/4	6528	8	3/1
1085	2	0/0	2446	4	3/2	3415	14	8/4	5512	5	1/1	6560	20	16/9
1122	10	3/1	2450	22	7/4	3436	5	4/1	5523	2	2/2	6576	18	11/5
1141	9	0/0	2533	49	9/1	3458	8	2/2	5526	34	34/14	6587	28	9/4
1157	10	8/2	2537	5	2/1	3480	1	1/1	5530	7	5/1	6593	20	13/2
1159	1	1/1	2586	11	7/7	3481	11	1/1	5548	9	8/4	6621	2	2/2
1190	4	2/2	2611	3	2/2	3488	6	6/5	5563	1	1/1	6629	6	4/3
1204	3	3/3	2628	7	5/2	3489	12	2/2	5567	5	1/1	6630	2	1/1
1385	23	4/1	2700	4	3/1	3491	3	1/1	5568	3	0/0	6665	8	2/1
1419	3	1/1	2736	1	1/1	3512	1	1/1	5572	3	3/3	6672	4	3/1
1425	7	5/1	2790	20	10/1	3516	10	7/2	5575	6	2/1	6683	10	10/3
1440	15	9/2	2793	7	4/3	3523	16	0/0	5591	10	7/4	6694	10	6/1
1443	2	2/2	2797	3	1/1	3569	4	2/2	5593	1	1/1	6764	8	3/1
1468	19	17/6	2798	11	1/1	3593	13	6/1	5601	1	1/1	6814	1	1/1
1533	32	20/12	2799	8	6/6	3598	3	3/2	5614	2	2/2	6816	8	7/3
1541	33	11/1	2812	15	12/9	3634	7	7/3	5621	6	3/1	6824	2	2/2
1578	3	0/0	2831	58	12/2	3648	3	3/1	5628	9	4/1	6904	1	1/1
1606	33	15/4	2852	23	5/1	3649	2	2/2	5644	4	1/1	6930	2	2/2
1609	8	2/1	2855	13	2/1	3658	4	2/1	5654	5	3/2	6963	17	10/2
1625	15	2/1	2856	86	19/3	3663	9	7/3	5704	9	8/4	7028	5	3/2
1652	6	1/1	2889	26	12/4	3765	4	2/2	5711	2	2/1	7113	52	8/1
1663	16	0/0	2891	18	15/4	3776	7	1/1	5725	13	12/6	7170	16	6/2
1664	5	1/1	2894	5	1/1	3788	4	3/1	5726	3	3/1	7172	1	1/1
1676	35	21/7	2913	5	2/2	3860	13	9/3	5773	4	1/1	7185	19	16/7
1683	6	3/1	2919	3	3/2	3866	1	1/1	5867	7	6/3	7240	4	4/4
1709	2	0/0	2929	44	16/5	3870	1	1/1	5955	4	2/2	7247	2	1/1
1711	8	2/1	2953	6	2/2	3891	3	2/1	5989	8	7/5	7255	5	1/1
1815	10	5/2	2958	2	2/2	3893	3	1/1	5995	7	1/1	7290	1	1/1
1883	1	1/1	2984	22	16/6	3905	4	4/1	6090	3	1/1	7301	51	13/7
1886	5	0/0	2988	2	2/2	3912	1	1/1	6100	3	0/0	7305	3	3/3

9 and Fig. 10. The distributions are very broad and the values of the best lognormal fits to the data are listed in Table 2. The lognormal distribution is compatible with the pulse areas and the amplitudes.

3.2.4. Time intervals between pulses

The distribution of the time intervals between the pulses is given in Fig. 11. The peak in the distribution occurred at about 1.0 s and was truncated at short time intervals by the 64 ms resolution of the data (Fig. 11a). A minimum time interval of 128 ms is required because two maxima

must be separated by at least one time bin. There could be a large additional excess of pulses with separations below the 128 ms resolution of the data that were not resolved. Other studies using different statistical methods from those employed here (Panaitescu et al., 1999; Lee et al., 2000a,b; Spada et al., 2000) have also noted a deficit of time intervals below one second. A parent lognormal distribution of time intervals with parameters similar to the observed distribution was simulated and the time intervals between the pulses recorded with an accuracy of 64 ms. The resulting distribution is given in Fig. 11a and the values of μ and σ for the parent distribution are given

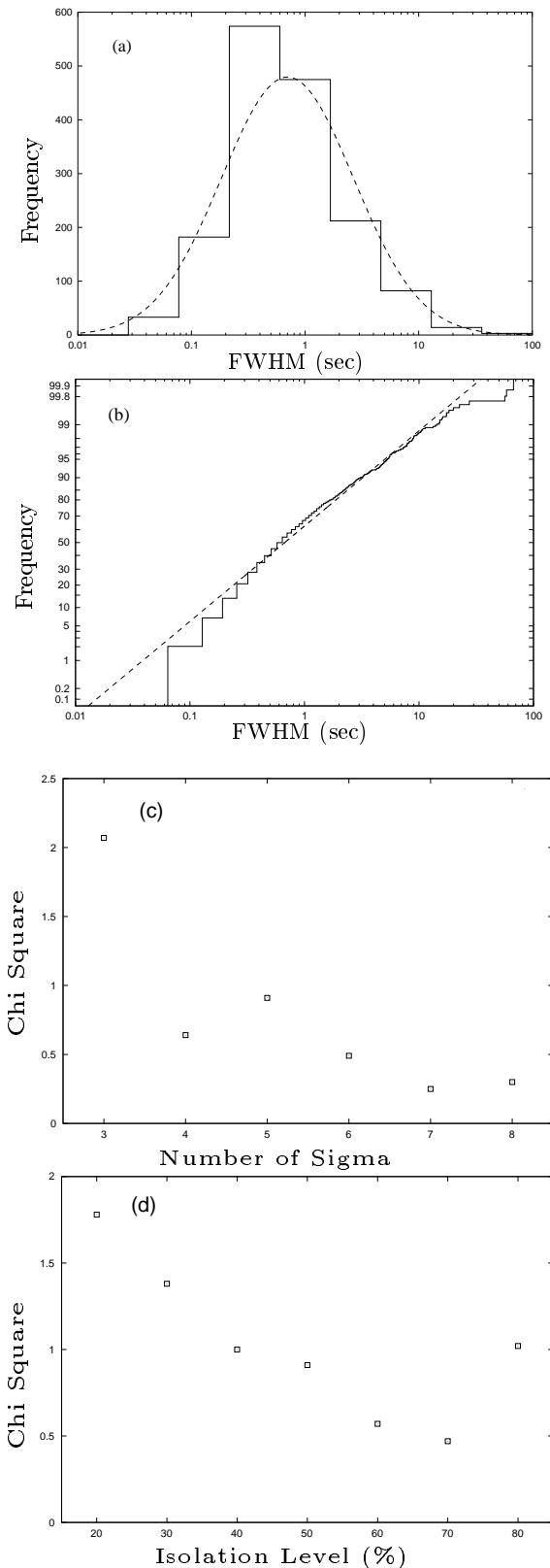


Fig. 6. (a) The distribution of the FWHM of pulses with $\tau_\sigma \geq 5$ and $\tau_I \geq 50\%$ and the best lognormal fit to the data. (b) The same data plotted as a cumulative percent such that a lognormal distribution yields a straight line. The large count in the first bin is due to the 64 ms time resolution. (c-d) The values of reduced χ^2 for the best lognormal fit as a function of τ_σ and τ_I .

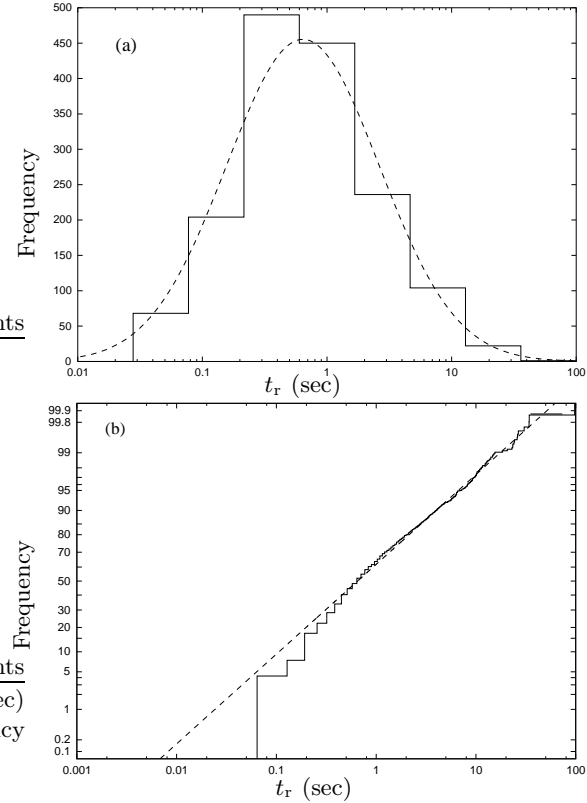


Fig. 7. (a) The distribution of the pulse rise times with $\tau_\sigma \geq 5$ and $\tau_I \geq 50\%$ and the best lognormal fit to the data. (b) The same data plotted as a cumulative percent. The large count in the first bin is due to the 64 ms time resolution.

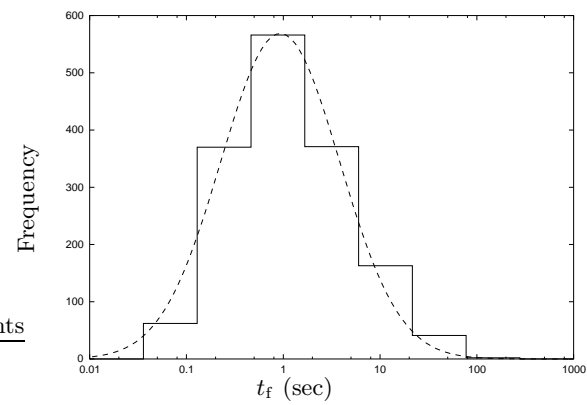


Fig. 8. The distribution of the fall times of the pulses with $\tau_\sigma \geq 5$ and $\tau_I \geq 50\%$ and the best lognormal fit to the data.

in Table 2. The measured distribution of time intervals in GRBs is consistent with the parent lognormal distribution provided a small (5%) excess of time intervals longer than 15 seconds is not included. This excess is clearly visible in Fig. 11a. The time intervals greater than 15 s are plotted in Fig. 11b. The data is well fit by a power law of slope -1.2.

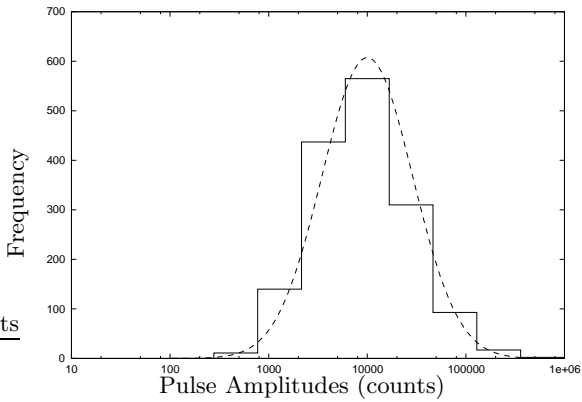


Fig. 9. The distribution of the pulse amplitudes with $\tau_\sigma \geq 5$ and $\tau_I \geq 50\%$ and the best lognormal fit to the data.

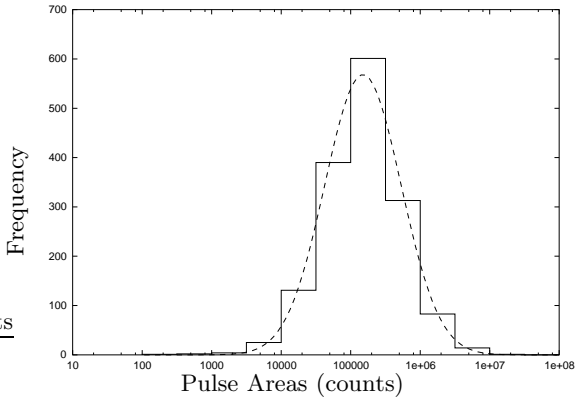


Fig. 10. The distribution of the pulse areas with $\tau_\sigma \geq 5$ and $\tau_I \geq 50\%$ and the best lognormal fit to the data.

Table 2. The parameters of the best lognormal fit. The parameters are expressed as natural logarithms, with the width of the distributions shown in normal space.

Property	μ	σ	χ^2	Width ($\pm 50\%$)
FWHM	-0.36	1.37	0.3	0.14 - 3.5
Rise time	-0.44	1.59	1.3	0.1 - 4.2
Fall time	-0.07	1.59	1.5	0.14 - 6.1
Pulse Amp.	9.0	1.12	0.3	$2.2 \times 10^3 - 30 \times 10^3$
Area	11.9	1.2	1.1	$35 \times 10^3 - 600 \times 10^3$
Time Int. ^a	0.21	1.03	—	0.37-4.14
Peak Energy ^b	5.6	0.58	—	137-535

^a See Sect. 3.2.4

^b See Sect. 3.2.5

3.2.5. Peak Energies

The values of the peak energy, E_{peak} , of a large sample of GRBs are given by Preece et al. (2000). There is an overlap of 77 GRBs with our sample, and the distribution of the values of E_{peak} for each section of these bursts are given in Fig. 12. The distribution was well fit by a lognormal distribution with a small tail noticeable at low

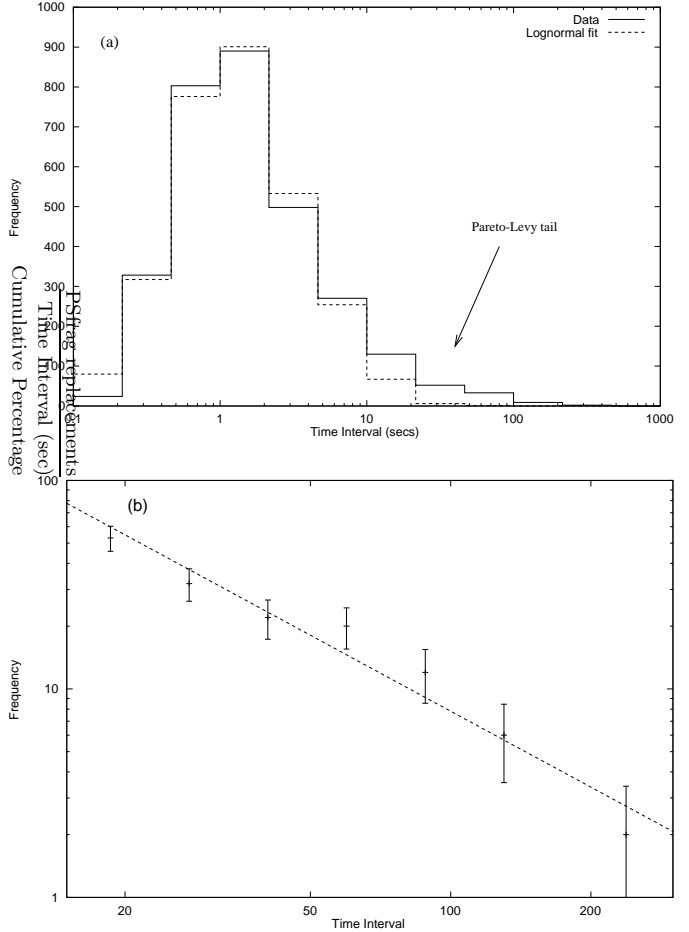


Fig. 11. (a) The measured distribution of time intervals between all the pulses and the best fit lognormal (dashed line) with allowance for the BATSE resolution of 64 ms. The excess of time intervals > 15 s is called the Pareto Lévy tail. (b) The Pareto tail of the time intervals is well fit by a power law (dashed line) of slope ~ -1.2 .

values of E_{peak} . The values of μ and σ are given in Table 2. The distribution of E_{peak} is noticeably narrower than that of the pulse parameters and spans a range of about 4 in width.

3.3. Summary

The major result of this part of the analysis is that the distributions of the rise times, fall times, FWHM, pulse amplitudes, pulse areas and the time intervals between the pulses are all very similar. The frequency distributions are very broad and cover about three orders of magnitude and all are compatible with the lognormal distribution. Li & Fenimore (1996) also showed that the pulse fluences and the time intervals between pulses are lognormally distributed for individual bursts in a small sample of bursts with more than 20 pulses. They also scaled the bursts to the same μ and σ and showed that the summation of all the peak fluences and time intervals looked lognormal, although no significance level was given for the

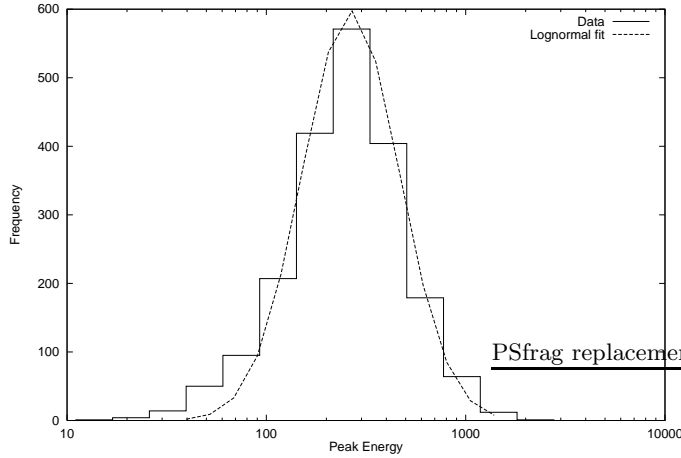


Fig. 12. The distribution of the peak energies and the best lognormal fit to the data (dashed line).

result. No normalisation of pulse properties was applied to the GRBs in this analysis, because only the brightest 319 bursts which had the best signal to noise ratio were analysed. From the data available for those bursts with known redshifts (Atteia et al., 1999), there does not appear to be any dependable standard by which to scale the bursts because of the broad range of intrinsic luminosities and their comparatively small range of distances. Therefore, to avoid introducing further biases, and to use all of the pulse information available, the data were analysed without scaling. However, as a test of this process, the data were also scaled and the same analysis performed on the scaled data, and no significant differences were found between the two data sets.

3.4. Correlations between burst and pulse parameters

It is important to determine how N relates to the other parameters of the GRB. In Fig. 13 N is plotted versus burst duration (T_{90}), total fluence and the median value of E_{peak} . Spearman rank order correlation co-efficients ρ and associated probabilities were obtained for the quantities in Fig. 13. The values are listed in Table 3 which also includes an additional range of burst parameters. The parameter C_{max} is the maximum value of the peak amplitude in that burst. The high values of ρ show a strong correlation between N and the total fluence, T_{90} and E_{peak} .

The values of ρ are not always uniformly distributed within each burst category. T_{90} versus fluence is much better correlated for category N than either O or P. N versus C_{max} and N versus HR are better correlated for category P than either N or O.

The Spearman rank order correlation coefficients and probabilities were evaluated for isolated pulses with the range of pulse parameters given in Table 4. The pulse parameters are strongly correlated with each other. The pulse amplitude is negatively correlated with the pulse rise and fall times and FWHM. In general the correlations are

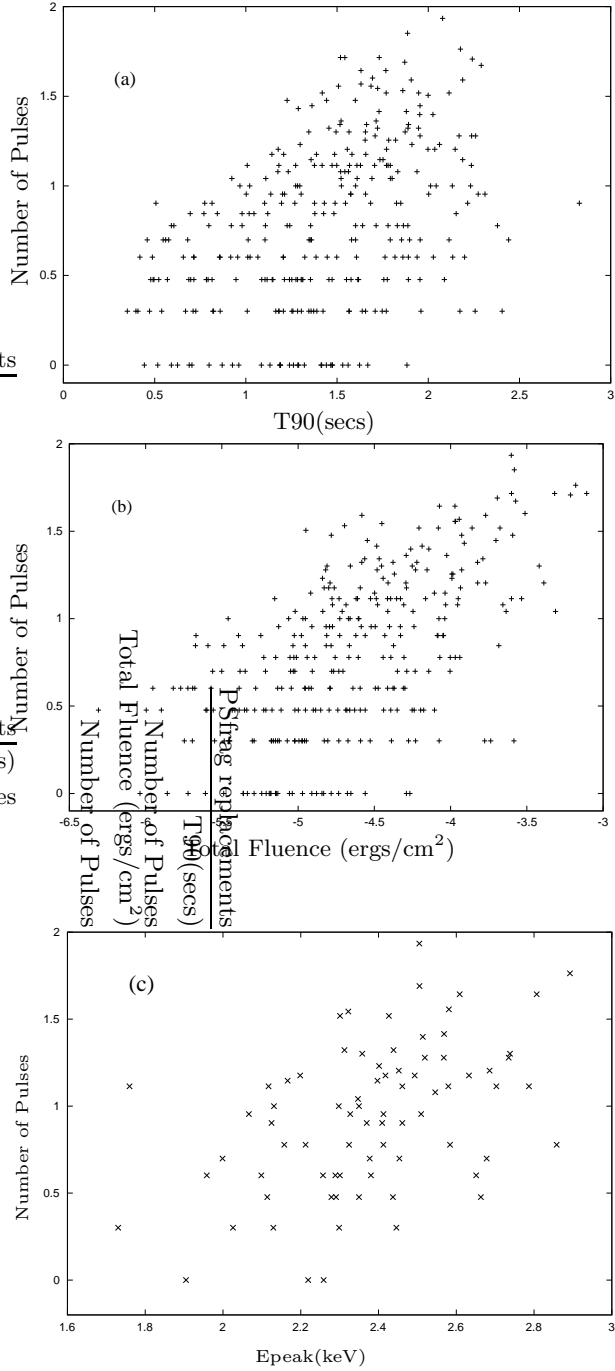


Fig. 13. The number of pulses in a GRB as a function of (a) T_{90} (b) total fluence and (c) the median value of the peak energy of the GRB. Quantisation occurs in the figures for low values of N .

stronger for categories M and N than either O or P. The only significant exception to this trend is the pulse amplitude versus area which also has the highest values of ρ for categories O and P.

Table 3. Spearman rank order correlation coefficients between a range of burst parameters

Properties	ρ	Probability
N vs. T_{90}	0.45	5×10^{-17}
N vs. Total Fluence	0.58	3×10^{-30}
N vs. C_{max}	0.27	6×10^{-7}
N vs. Hardness Ratio	0.29	1.2×10^{-7}
N vs. E_{peak}	0.49	7×10^{-6}
T_{90} vs. Total Fluence	0.52	6×10^{-24}
T_{90} vs. C_{max}	-0.08	0.16
T_{90} vs. Hardness Ratio	0.11	0.05
Total Fluence vs. Maximum Pulse	0.48	1.3×10^{-15}
Total Fluence vs. Hardness Ratio (HR)	0.56	3×10^{-27}
C_{max} vs. HR	0.25	4.4×10^{-6}

Table 4. Spearman rank order correlation coefficients between a range of pulse parameters.

Properties	ρ	Probability
Rise Time vs. Fall Time	0.64	$< 10^{-48}$
Rise Time vs. FWHM	0.65	$< 10^{-48}$
Rise Time vs. Pulse Area	0.34	2.9×10^{-34}
Rise Time vs. Pulse Amplitude	-0.27	1.9×10^{-21}
Fall Time vs. FWHM	0.70	$< 10^{-48}$
Fall Time vs. Pulse Area	0.42	$< 10^{-48}$
Fall Time vs. Pulse Amplitude	-0.22	1.4×10^{-14}
FWHM vs. Pulse Area	0.44	$< 10^{-48}$
FWHM vs. Pulse Amplitude	-0.27	2.7×10^{-21}
Pulse Area vs. Pulse Amplitude	0.63	$< 10^{-48}$
FWHM vs. Time Interval	0.58	10^{-48}

3.5. Correlations between the time intervals between pulses and pulse amplitudes

Spearman rank order correlation coefficients and probabilities were evaluated for the time intervals between pulses (ΔT) with $\tau_\sigma > 5$. The results are presented in Table 5 for two cases (1) the time intervals were not normalised and (2) the time intervals were normalised to T_{90} . There is a good correlation between the time intervals in both cases that declines slowly with increase in the number of time intervals. The largest values of ρ occurred in category N.

The Spearman correlation coefficients were also evaluated between pulse amplitudes and the results are given in Table 6 for two cases (1) the amplitudes were not normalised and (2) normalised to the largest amplitude pulse in the burst. The normalised pulse amplitudes are less strongly correlated over many pulses than the time intervals. These results were obtained for all pulses with $\tau_\sigma \geq 5$ and without satisfying any selection based on pulse isolation. The role of pulse pile-up has yet to be investigated.

3.6. The properties of the pulses as a function of, N, the number of pulses in the GRB

It was noticed early in this analysis that pulse properties depended strongly on N (Quilligan et al., 2000). The median value of the isolated pulse timing parameters were

Table 5. Spearman rank order correlation coefficients ρ for time intervals between pulses. The two values for ρ and the probability are for unnormalised/normalised time intervals.

Number of Intervals	Total Number	ρ	Probability
1	2751	0.42/0.56	$< 10^{-48}$
2	2499	0.34/0.48	$< 10^{-48}$
5	1929	0.24/0.37	$5 \times 10^{-26} / < 10^{-48}$
10	1395	0.20/0.29	$3 \times 10^{-13} / 6 \times 10^{-27}$
15	890	0.16/0.25	$3 \times 10^{-6} / 4 \times 10^{-14}$
20	634	0.10/0.23	$8 \times 10^{-3} / 3 \times 10^{-9}$
25	459	0.08/0.22	$7 \times 10^{-2} / 1 \times 10^{-6}$
30	322	0.03/0.14	$3 \times 10^{-2} / 10^{-2}$

Table 6. Spearman rank order correlation coefficients ρ and associated probabilities for the pulse amplitudes. The two values for ρ and the probability are for unnormalised/normalised amplitudes.

Number of Amplitudes	Total Number	ρ	Probability
1	3039	0.72/0.57	$< 10^{-48}$
3	2499	0.55/0.32	$< 10^{-48}$
5	2098	0.52/0.24	$< 10^{-48} / 3 \times 10^{-29}$
7	1777	0.48/0.15	$< 10^{-48} / 6 \times 10^{-11}$
9	1510	0.43/0.08	$< 10^{-48} / 2 \times 10^{-3}$
10	1395	0.44/0.08	$< 10^{-48} / 3 \times 10^{-2}$

determined for all GRBs with the same value of N. The median values of the rise time, fall time, FWHM and time interval between pulses are plotted versus N in Fig. 14(a-d). The largest value usually occurred for N = 1 or 2 and subsequently declined significantly as N increased. There are some values that are well removed from the general trend but they usually have a small number of pulses. The median values of the area and amplitude for isolated pulses are given in Fig. 15 (a-b). The trend is quite different from Fig. 14. The amplitude is reasonably constant up to N ~ 35 with a clear increase for higher values of N. There is a similar but weaker trend for the pulse area which has the largest value at N = 1.

The properties of the four categories of GRBs are summarised in Table 7. The median values of the pulse timing parameters all decrease by at least a factor of four from category M to P. In contrast the median values of T_{90} , total fluence, hardness ratio and maximum pulse amplitude all increase significantly. The median variability, is defined as the number of pulses $\geq 5 \sigma$ divided by the time the emission is $\geq 5 \sigma$, also increases from category M to P.

3.7. First Half/Second Half analysis

To study the evolution of the time profile as the GRB progresses, each GRB was divided into two, to include the pulses that occur before and after the strongest pulse

Table 7. The properties of the four categories of pulses in GRBs. The last five entries are for the 250 GRBs that were summed over two detectors.

GRB Category	M	N	O	P
Number of Pulses per GRB	1-2	3-12	13-24	25+
Number of GRBs	67	162	56	34
Total number of pulses	103	981	933	1341
Number of isolated pulses at 50% level	83	522	476	494
Median T_{90} (sec)	18.1	20.4	45.7	58.7
Median Total Fluence (ergs/cm ²)	8.8×10^{-6}	1.7×10^{-5}	4.2×10^{-5}	1.2×10^{-4}
Median hardness ratio (Chan $\frac{4+3}{2+1}$)	3.4	4.1	6.5	8.3
Median C_{max} (ph/cm ² /sec)	4.7	6.1	9.3	12.6
Median Variability	0.09	0.29	0.39	0.53
Median Rise Time (sec)	1.7	0.8	0.64	0.45
Median Fall Time (sec)	5.2	1.5	1.0	0.7
Median FWHM (sec)	1.8	0.7	0.64	0.45
Median Time Interval (sec)	4.8	1.9	1.5	1.0
Number of GRBs	55	130	38	27
Total number of pulses	87	778	648	1081
Number of isolated pulses at 50% level	70	416	319	404
Median Pulse Amplitude (Iso. pulses) (counts)	13×10^3	7.3×10^3	7.3×10^3	9.5×10^3
Median Area (counts)	560×10^3	180×10^3	140×10^3	140×10^3

Table 8. Summary of the first half/second half analysis of the three categories of the GRBs.

GRB Category	N	O	P
Number of Pulses per GRB	3-12	13-24	25+
Total Number of Pulses (1st/2nd half)	404/415	384/493	679/628
Total Number of Isolated Pulses (50%) (1st/2nd half)	193/220	182/261	203/271
Total Number of Isolated Pulses (75%) (1st/2nd half)	79/126	77/101	71/83
Median Rise Time (1st/2nd half)	1.02/0.70	0.77/0.58	0.51/0.45
K-S Statistic/Probability	0.13/5%	0.12/9%	0.11/11%
Median Fall Time (1st/2nd half)	1.09/1.89	0.90/1.22	0.70/0.70
K-S Statistic/Probability	0.20/.02%	0.15/2%	0.11/10%
Median Asymmetry Ratio (1st/2nd half)	1.0/0.4	0.75/0.49	0.75/0.54
K-S Statistic/Probability	$0.27/3 \times 10^{-5}\%$.17/0.3%	0.14/1.5%
Median FWHM (1st/2nd half)	0.77/0.67	0.64/0.64	0.51/0.45
K-S Statistic/Probability	0.08/55%	0.08/52%	0.11/11%
Median Time Interval (1st/2nd half)	1.60/2.10	1.41/1.54	1.02/1.02
K-S Statistic/Probability	0.13/2%	0.06/35%	0.05/30%
Median Pulse Amplitude ($\times 10^3$)(1st/2nd half)	6.2/5.4	7.3/6.8	18.1/11.2
K-S Statistic/Probability	0.09/41%	0.08/52%	0.09/25%
Median Area ($\times 10^3$)(1st/2nd half)	151/127	133/118	152/130
K-S Statistic/Probability	0.08/50%	0.07/59%	0.14/2%

in the burst. Only GRBs with more than two pulses are included, resulting in a reduced total sample of 252. The first half (pre-main pulse) of the GRB was compared with the second half (post-main pulse). The bursts are also subdivided into three categories. A summary of the properties of the GRBs used is given in Table 8.

The first half/second half analysis was performed on the three timing parameters of the pulses, time intervals between the pulses, amplitude, area and the pulse asymmetry ratio which is defined as the ratio of the pulse rise

time to the pulse fall time. The median values of the distributions in the three categories in the first half and second half analysis are given in Table 8 along with the results of the Kolmogorov-Smirnov (KS) tests. The KS probability is a measure of whether the two distributions (first/second half) are drawn from the same parent distribution.

The first result is that the median values of the timing parameters of the pulses and the time intervals between the pulses all decrease by an average of 1.8, from the category N to P including the first half and second half of

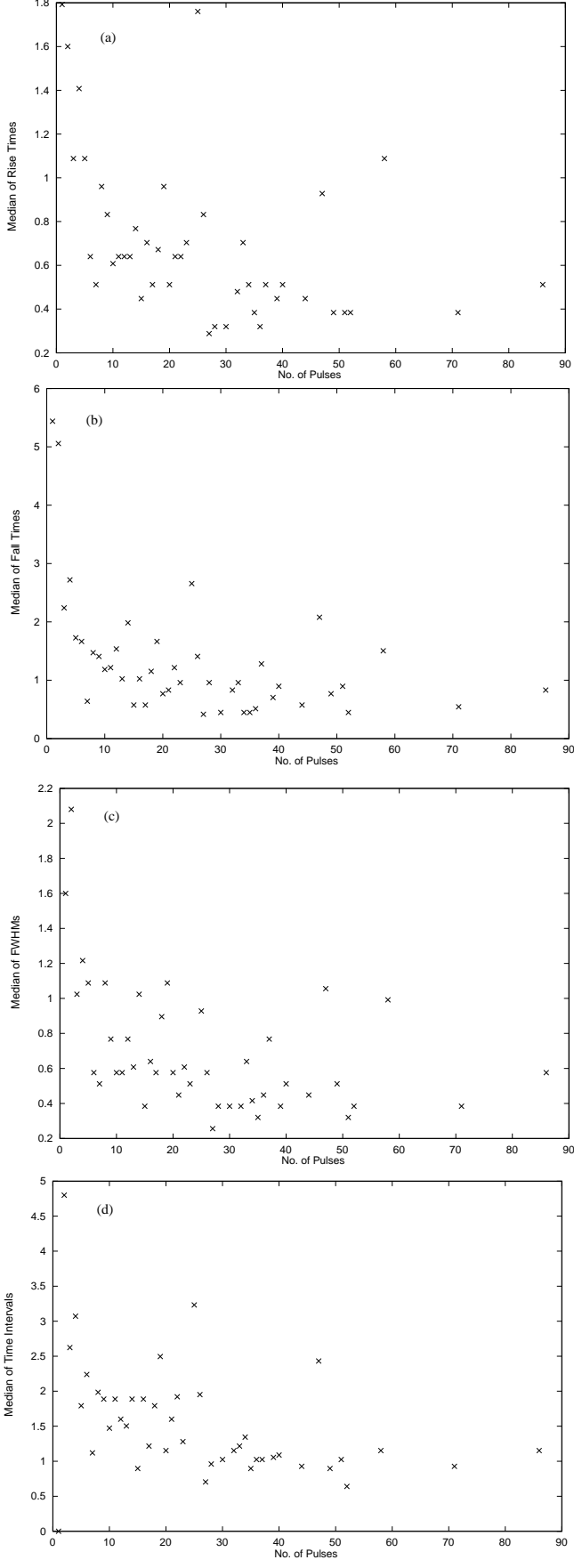


Fig. 14. The median values of (a) rise time, (b) fall time, (c) FWHM and (d) the time intervals between pulses versus the number of pulses

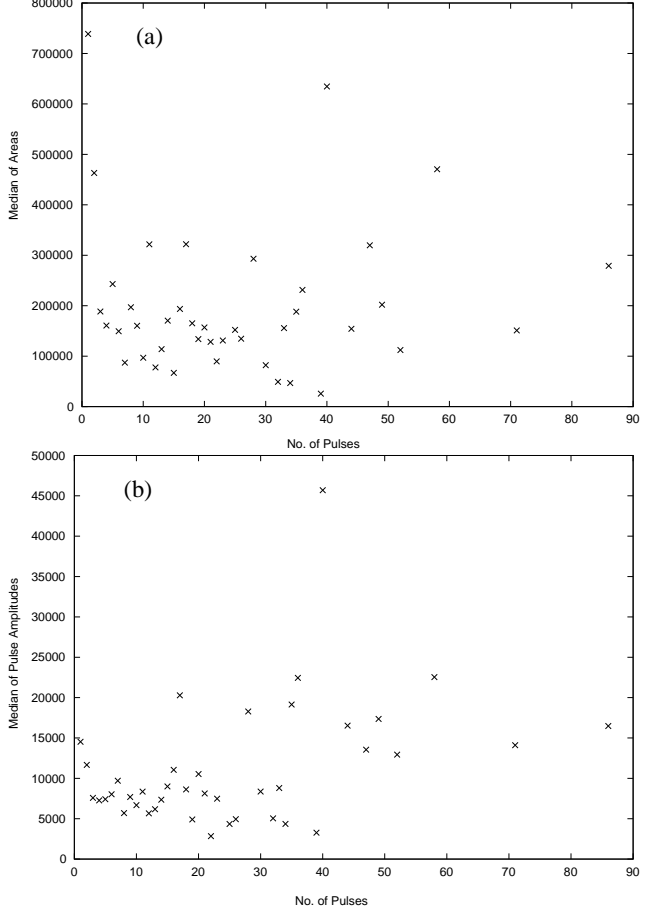


Fig. 15. The median values of (a) pulse area and (b) pulse amplitudes versus the number of pulses.

the GRBs. In the case of the rise times, the median values of the distributions decrease from 1.02 to 0.51 in the first half and 0.70 to 0.45 in the second half. The trend in the median value of the pulse amplitude is in the opposite direction with larger pulses in category P than either O or N.

In the first/second half analysis there is a trend in the three categories for the median rise time to be slower in the first half of the burst (1.02 versus 0.70 for category N). The difference could be caused by an additional clearing out effect at the start of the GRB. There is also a clear indication at the 0.02% level that the pulse fall time is faster in the first half than the second for category N (1.09 versus 1.89 for category N) and this effect weakens for categories O and P. The median values of the pulse asymmetry ratio also show the most significant differences for category N where the median values are 1.0 and 0.4 for the first and second halves. The KS test gives good agreement between the first half and second half for the FWHM, time intervals between pulses, the pulse amplitudes and areas. The median values of the pulse amplitude and areas are however larger in the first half than the second half for the three categories of GRBs.

4. Discussion

4.1. Pulse shapes in GRBs

A complete study of the BATSE time profiles of the brightest 319 GRBs has been presented. The statistical analysis of the data reveal the ubiquitous nature of the log-normal distribution in GRB time profiles (Figs. 6-10). The means and variances of the best fit lognormal functions are given in Table 2. The results presented in Figs. 6-10 are for the isolated pulses from the four GRB categories. The data in Table 7 and the first half/second analysis show that the median values of the pulse properties vary with N. Lognormal distributions also apply to the spectral properties of GRBs. The BATSE spectroscopic detectors revealed that the break energies in GRB spectra are compatible with a lognormal distribution (Preece et al., 2000). The FWHM of the distributions that describe the pulses are in the range 14-45 (Table 2) whereas the value for E_{peak} is only ≈ 4 and extends from 137 keV to 535 keV. The unexpected narrowness of the E_{peak} distribution is a major problem in GRBs (Brainerd, 2000). Furthermore, spectral fitting of 41 pulses in 26 GRBs showed that the spectral hardness parameter E_{peak} decays linearly with energy fluence and that the distribution of the decay constants is roughly lognormal (Crider et al., 1999).

The Spearman rank order correlation coefficients were obtained for a range of burst parameters (Table 3). There is good agreement with the results of Lee et al. (2000a) who used a different method. N is strongly correlated with total fluence, T_{90} , HR and E_{peak} (Fig. 13). N is an important quantity in determining GRB properties and provides the link between total fluence and duration since both increase with N. The correlation coefficients between the parameters that describe the pulses are given in Table 4. The rise and fall times, FWHM and area of the pulses are highly correlated. There is a high probability that a pulse with a fast rise time will also have a fast fall time and a short FWHM. The pulse amplitude is negatively correlated with the rise and fall times and FWHM. The anticorrelation between the pulse amplitude and pulse width has been observed in other studies (Lee et al., 2000a; Fenimore & Ramirez-Ruiz, 2001). The pulse width is also a function of energy and varies as $E^{-0.45}$ (Fenimore et al., 1995) and this effect has been attributed to synchrotron radiation (Piran, 1999). The FWHM is strongly correlated with the preceding and subsequent time interval between pulses (Table 4). This result is in agreement with Nakar & Piran (2001) and the prediction of the internal shock model. A further comparison of the pulse timing parameters, the energy dependence and the spectral lag may reveal further interesting constraints on the emission process (Norris et al., 2001; Daigne & Mochkovitch, 2001). The unique properties of the pulses in GRBs have been summarised by McBreen et al., (2002).

The lognormal distribution arises from a statistical process whose result depends on a product of probabilities arising from a combination of independent events. It

therefore identifies the statistical process but not the combination of events that lead to the formation of the pulse shape and the peak energy. In the internal shock model the main factors contributing to the pulse shape include (Rees & Mészáros, 1994; Piran, 1999).

1. the Lorentz factors, masses and thickness of the interacting shells
2. the distance from the central engine and curvature where the collisions occur
3. the energy conversion in the shock, the nature of the magnetic field and particle acceleration process
4. the synchrotron radiation mechanism possibly modified by self-absorption and pair production
5. the time scale for energy loss by the particles.

The resulting properties of the pulses in GRBs depend on a combination of many events and hence it is not surprising that the lognormal distribution gives an elegant description of all their properties. Random multiplicative processes abound in a variety of natural phenomena and a good example is the statistical description of the strokes in flashes of lightning. Almost all the properties of the strokes in the flashes and the flashes themselves are well described by lognormal distributions (Uman, 1987; McBreen et al., 1994).

4.2. Time intervals between pulses in GRBs

It is often found that distributions that seem to be lognormal over a wide range change to an inverse power law distribution for the last few percent. An amplification model has been used to characterise the transition from a lognormal distribution to a power law that is often called a Pareto-Lévy tail (Montroll & Shlesinger, 1982). The distribution of time intervals conform to the lognormal distribution over most of the range with the exception of about 5% of the time intervals longer than about 15 s (Fig. 11). The Pareto-Lévy tail of time intervals have an amplification process that is not available to most time intervals.

The origin of the nonrandom distribution of time intervals between pulses is an important clue to the GRB process. In the internal shock model there is almost a one to one correspondence between the emission of shells and pulses resulting from the collisions of shells (Kobayashi et al., 1997). Hence the time intervals between pulses is an almost direct measure of the activity of the central engine. The temporal behaviour of soft gamma-ray repeaters and young pulsars provide additional context in which to view the results of GRB time profiles. The time intervals between about 30 microglitches in the Vela Pulsar are consistent with a lognormal distribution with a mean of 50 days (Hurley et al., 1994, 1995; Cordes et al., 1988). The amount of energy involved in the microglitches is about 10^{38} ergs. The macroglitches in the Vela Pulsar are about a thousand times more powerful but occur too infrequently to determine the distribution of time intervals but they have a wide range and do not seem inconsistent with the lognormal distribution. More energetic out-

bursts have been recorded from SGR sources. The two most energetic events released about 5×10^{44} ergs in γ -rays from SGR 0526-66 on 5 March 1979 (Mazets et al., 1979) and about 10^{43} ergs from SGR 1900+14 on 27 August 1998 (Hurley et al., 1999). The SGR sources also generate a large number of smaller outbursts, and it has been shown that the time intervals between outbursts are distributed lognormally (Hurley et al., 1994; Gögiüs et al., 2000). Hence lognormally distributed time intervals between outbursts and glitches are characteristic features of SGR sources and neutron star microglitches. It is widely accepted that these sources are rotating neutron stars with high magnetic fields. It is not unreasonable to argue that the coupled effects of rapid rotation and intense magnetic fields (Klužniak & Ruderman, 1998) are also involved in powering GRBs since the time intervals between pulses are also consistent with a lognormal distribution.

The possibility that a rapidly rotating neutron star with a surface magnetic field of $\sim 10^{15}$ Gauss could power a GRB has been suggested (Usov, 1992). Once formed such a neutron star could lose its rotational energy catastrophically on a time scale of seconds. The rotation of the star decelerates because of the applied torques. Powerful transient fields may also occur in the merger of two neutron stars or a neutron star and a black hole. The energy stored in differential rotation of the collapsed object would be released in sub-bursts as toroidal magnetic fields are repeatedly wound up to $\sim 10^{17}$ Gauss (Klužniak & Ruderman, 1998). The emergence of a toroid is accompanied by huge spin down torques, the reconnection of new surface magnetic fields and rapid release of a sub-burst of energy of about 10^{51} ergs. The release of rotational energy in repeated sub-bursts could power the GRB. If the differentially rotating compact object forms a torus about a spinning black hole either in a merger or core collapse of a massive star, energy can be extracted by the magnetic field that threads the torus and the black hole (Mészáros, 2001). As the torus builds up and ejects its magnetic toroids, the differential rotation of the torus could be maintained by the spin of the black hole. The models of GRBs with the coupled effects of rapid rotation and ultra intense magnetic fields are particularly attractive because the time intervals between pulses in GRBs are distributed lognormally and follow the pattern observed in non-catastrophic events in SGRs and pulsars.

The time intervals between the pulses are correlated with each other and the correlation decreases slowly with increase in the number of time intervals (Table 5). This effect had previously been observed in a small sample of GRBs (Nakar & Piran, 2001) and attributed to the internal shock model. In addition the pulse amplitudes are also correlated with each other and this effect decreases more rapidly than the time intervals between pulses (Table 6). Similar correlations have been found between the pulse amplitudes and also time intervals between pulses in short GRBs (McBreen et al., 2001). In the internal shock model, these correlations originate in the central engine and provide strong constraints on any viable model of GRBs.

GRB models leave open many possibilities to account for the Pareto-Lévy tail of long time intervals. The excess of long time intervals have been noted in other studies (Ramirez-Ruiz & Mervoni, 2001; Nakar & Piran, 2001). The properties of the GRBs with long time intervals will be covered in a separate publication.

4.3. Numbers of pulses and jets in GRBs

A detailed comparison has been made between the distributions of the properties of the pulses in the first half and second half for three categories of GRBs. There are no statistically significant differences between the median values of the time intervals between pulses, pulse amplitude, areas and FWHM in the first half and second half of GRBs (Table 8). There are two trends in the pulse rise times and fall times that should be noted: 1) the median rise time is slower in the first half for the three categories of bursts (Table 8) and 2) the median fall time is faster in the first half for categories N and O. The combination of slower rise times and faster fall times gives a pulse asymmetry ratio with a significant difference between the first half and second half for category N and at a reduced significance level for O and P (Table 8). The effect could be caused by a clearing out process such as additional baryon loading or Compton drag in the first half of the bursts with small number of pulses. These results are also compatible with the constancy of the pulse widths observed by Ramirez-Ruiz & Fenimore (2000) using a peak aligned profile method on a small sample of GRBs with more than 20 pulses. In the internal shock model, the rapid variability in GRB time profiles is due to emission from multiple shocks in a relativistic wind (Piran, 1999; Panaitescu et al., 1999; Downes et al., 2001). The temporal position of the pulse is unconnected to the collision parameters and in this way the little or no evolution of the pulses in GRBs can be explained (Fenimore & Ramirez-Ruiz, 2001). The rise time and fall time may be determined by the hydrostatic time $\approx d/c$ and the angular spreading time $\approx D/c$, where d and D are the width and separation of the shells (Kobayashi et al., 2001). The observed evolution of the pulses requires the shells to be narrower and farther apart later in the GRB. This prediction is in agreement with the data because the time intervals between pulses are longer in the second half of the burst (Table 8).

However, it is evident from Figs. 14 and Tables 7 and 8 that as the number of pulses in a burst increases, the median values of the rise and fall times, FWHM and time intervals all decrease and by about the same amount. The GRBs with more pulses also have on average significantly longer durations, higher fluences and hardness ratios (Table 7). The variability index of a GRB was taken to be the number of pulses $\geq 5\sigma$ divided by the time the GRB emission was also $\geq 5\sigma$. The median values are given in Table 9 for the four GRB categories. The GRBs with more pulses have a higher variability index. These results provide an interesting interpretation of the two cor-

relations that have been reported for GRBs with known redshift: (1) the more luminous GRBs to be more variable (Fenimore & Ramirez-Ruiz, 2001) and (2) there is an anticorrelation between the arrival times of high energy and low energy pulses in GRBs (Norris et al., 2000; Salmonson, 2000). Recently Schaefer et al. (2001) showed that there is a relationship between the variability and spectral lag (Ioka & Nakamura, 2001). There is a good correlation between the values of the variability obtained here and those of Fenimore & Ramirez-Ruiz (2001). GRBs with higher values of HR have lower values of $\langle V/V_{\max} \rangle$ implying they are a more distant and luminous population (Schmidt, 2001).

Our knowledge on the shape of the emitting region in GRBs is restricted because, due to relativistic beaming, only a small portion of angular size $\sim \Gamma^{-1}$ is visible to the observer. Thus the observer is unable to distinguish a sphere from a jet as long as $\Gamma > \theta^{-1}$ where θ is the radius of the opening angle of jet (Rhoads, 1997). However as the source continues its rapid expansion, Γ will decrease, and when $\Gamma < \theta^{-1}$ there will be a marked decrease in the observed flux. The steep time dependence of the afterglow emission, sometimes with changes in the slope of the spectrum, and radio emission have been widely interpreted as evidence for emission from jets (Castro-Tirado, 2001; Mészáros, 2001; Frail et al., 2001). The GRBs with more pulses appear to have higher values of the Lorentz factor Γ . The higher values of Γ may come from a more efficient and more active central engine. In one variation of the internal shock model, it was assumed that the degree of collimation of the jet depended on the mass M at the explosion (Kobayashi et al., 2001). A wide jet involves a large mass that results in a flow with a lower Γ . The pulse properties depend strongly on $\Gamma_{\min}, \Gamma_{\max}$ and the radius of the photosphere R_{\pm} . GRBs with faster pulses originate in collisions above R_{\pm} whereas GRBs with slower pulses have smaller values of Γ and some collisions below the photosphere. While this homogeneous model may explain pulse properties in GRBs, the strong possibility of inhomogeneous jets with a variable Γ should also be examined.

Baryon loading can be a major problem in GRB models and severely limit the attainable value of Γ (Rees, 1999; Mészáros et al., 1998; Salmonson, 2000). There maybe a broad range of Γ 's in the outflow with the highest value occurring close to the rotation axis where the baryon contamination should be at a minimum. At larger angles from the axis, there may be an increasing degree of contamination with a corresponding drop in Γ . The outcome of a collapse in a massive star whose iron core collapsed to a black hole have been computed (MacFadyen & Woosley, 1999). The resulting jet that drives out through the star is probably powered by a MHD process which can in principle convert a large portion of the binding energy at the last stable orbit into jet energy. The large amount of energy dumped into the natural funnel-shaped channel creates a highly collimated jet, focused into a small region of the sky. The largest value of Γ occurs on axis and decreases with increasing θ because the material coming at the ob-

server has less energy at larger angles. The emission is still beamed into an angle Γ^{-1} but in this inhomogeneous model the angle varies across the opening angle of the jet (Rossi, Lazzati & Rees, 2001). In this situation the properties of the pulses in GRBs can be influenced by the jet. The BATSE sample of the brightest GRBs should contain a range of angles within the jet and hence different values of Γ . In this context it is reasonable to identify the complex GRBs with more pulses and higher values of Γ with angles near the axis of jet. The GRBs that are viewed at larger angles from the jet axis have on average lower values of Γ , and develop at the greater distances from the central engine and should have slower pulses.

In this context it is interesting to note that the pulse evolution consisting of slower rise times and faster fall times in the first half, is more pronounced for GRBs in category N than either O or P. In a jet model with a variable Γ , the GRBs in category N would be on average farther from the axis and more sensitive to a clearing out effect such as additional baryon loading or Compton drag (Rees, 1999; Ghisellini, 2001) in the initial phase of the GRB.

The steep and variable slope of the decay of GRB afterglows have been widely interpreted as evidence for jets in GRBs (Mészáros, 2001; Castro-Tirado et al., 2001). If the axis of the jet is pointed close to the observer, the GRB will be intense and the afterglow should contain evidence for good alignment. It is interesting that the two brightest GRBs detected by WFC on BeppoSAX also were the best aligned. The recent detection of a bright GRB with a fluence of 10^{-4} ergs cm^{-2} also had a very bright afterglow (Castro-Tirado et al., 2001). However many more GRBs and afterglows are required to verify the existence of a pattern between the strongest GRBs and their afterglows (Frail et al., 2001). The distribution of the number of pulses per GRB (Fig. 5) may broadly represent the beaming by the jet because bursts with large numbers of pulses and higher variability (Table 7) may be close to the axis and bursts with smaller numbers of pulses and less variability further off-axis.

5. Conclusions

The properties of the brightest 319 GRBs in the BATSE current catalogue have been analysed. The automatic pulse selection process detected more than 3300 pulses. The distributions of pulse rise and fall times, FWHM, areas, amplitudes and time intervals between pulses are reasonably consistent with the lognormal distribution. GRB pulse profiles can be elegantly described by a small number of parameters that may be very useful for simulations. The lognormal distribution depends on the product of probabilities arising from a combination of independent events and these conditions must therefore apply to the generation of the temporal and spectral properties of GRB pulses. A wide range of burst parameters and also pulse parameters were correlated and the results follow the trend expected from the internal shock model. The pulse

amplitude is strongly anticorrelated with the other pulse timing parameters. The time intervals between pulses and pulse amplitudes are correlated with each other.

A comprehensive analysis has been performed between the first half and second half of GRBs in three categories defined in terms of N . No major differences were found between the distribution of pulse properties between the first half and second half of the GRBs. There is a strong tendency for pulses to have slower rise times and faster fall times in the first half of the burst. This trend is stronger in GRBs with small numbers of pulses. The pulse timing parameters and time intervals all decrease with increase in N . These results seem to be compatible with jet models with either a Γ that varies with the opening angle or is constant and varies with the mass. If Γ varies with the opening angle of the jet, the GRBs with higher values of Γ and greater variability are observed close to the axis of the jet while GRBs with smaller number of pulses and less variability are observed at larger angles from the jet. Jets with values of Γ that vary with angle or with mass may explain the luminosity-variability correlation and the luminosity-energy lag correlation in GRBs with known redshift.

This study of the number of pulses in GRBs and their time structure provides strong evidence for rotation powered systems with intense magnetic fields and the added complexity of a jet. These results can be well interpreted by internal shocks in the framework of theoretical models for the formation of black holes and subsequent jet formation.

References

Aitchison, J. & Brown, J. A. C. 1957, *The Lognormal Distribution* (Cambridge: Cambridge University Press)

Arneodo, A., Manneville, S., Muzy, J. F., & Roux, S. G. 1999, *Phil. Trans. R. Soc. Lond. A*, 357, 2415

Atteia, J., Boér, M., & Hurley, K. 1999, *A&AS*, 138, 421

Band, D., Matteson, J., Ford, L. et al. 1993, *ApJ*, 413, 281

Belli, B. M. 1992, *ApJ*, 393, 266

Beloborodov, A. M., Stern, B. E., & Svensson, R. 2000, *ApJ*, 535, 158

Berger, E. A., Kulkarni, S. R., & Frail, D. A. 2001, [astro-ph/0105081]

Bhat, P. N., Fishman, G. J., Meegan, C. A. et al. 1994, *ApJ*, 426, 604

Borgonovo, L., Ryde, F. 2001, *ApJ*, 548, 770

Brainerd, J. J. 2000, *ApJ*, 538, 628

Castro-Tirado, A. J. 2001, [astro-ph/0102122]

Castro-Tirado, A. J., Sokolov, V. V., Gorosabel, J. et al. 2001, *A&A*, 370, 398

Chang, H. & Yi, I. 2000, *ApJ*, 542, L17

Cordes, J. M., Downs, G. S., & Krause-Polstorff, J. 1988, *ApJ*, 330, 847

Costa, E., Frontera, F., Heise, J. et al. 1997, *Nature*, 387, 783

Crider, A., Liang, E. P., Preece, R. D. et al. 1999, *Ap&SS*, 138, 401

Daigne, F. & Mochkovitch, R. 1998, *MNRAS*, 296, 275

Daigne, F. & Mochkovitch, R. 2001, *Proceedings of Gamma-Ray Burst and Afterglow Workshop*, Woods Hole, November 5-9 (In press)

Daubechies, I. 1992, *Ten Lectures on Wavelets* (Philadelphia: Capital City)

Dermer, C. D. & Mitman, K. E. 1999, *ApJ*, 513, L5

Downes, T. P., Duffy P., & Komissarov, S. 2001, *MNRAS*, pg.275

Eichler, D., Livio, M., Piran, T., & Schramm, D. N. 1989, *Nature*, 340, 126

Fenimore, E. E., in 't Zand, J. J. M., Norris, J. P., Bonnell, J. T., & Nemiroff, R. J. 1995, *ApJ*, 448, L101

Fenimore, E. E. & Ramirez-Ruiz, E. 2001, *ApJ*, submitted, [astro-ph/0004176]

Frail, D. A., Kulkarni, S. R., Sari, R., et al. 2001, *Nature*, in press

Fryer, C. L., Woosley, S. E., Herant, M., & Davies, M. B. 1999, *ApJ*, 520, 650

Ghisellini, G. 2001, [astro-ph/0105052]

Gögüs, E., Woods, P. M., Kouveliotou, C. et al. 2000, *ApJ*, 532, L121

Golenetskii, S. V., Mazets, E. P., Aptekar, R. L., & Ilinskii, V. N. 1983, *Nature*, 306, 451

Hanlon, L., Laureijs, R. J., Metcalfe, L. et al. 2000, *A&A*, 359, 941

Hurley, K., Cline, T., Mazets, E. et al. 1999, *Nature*, 397, 41

Hurley, K. J., McBreen, B., Delaney, M., & Britton, A. 1995, *Ap&SS*, 231, 81

Hurley, K. J., McBreen, B., Quilligan, F., Delaney, M., & Hanlon, L. 1998, in *CP428, Gamma-Ray Bursts, 4th Hunstville Symposium*. Edited by C.A. Meegan et al., 191

Hurley, K. J., McBreen, B., Rabbette, M., & Steel, S. 1994, *A&A*, 288, L49

Ioka, K. & Nakamura, T. 2001, *ApJ*, 554, L163

Kluźniak, W. & Ruderman, M. 1998, *ApJ*, 508, L113

Kobayashi, S., Piran, T., & Sari, R. 1997, *ApJ*, 490, 92

Kobayashi, S., Ryde, F., & MacFadyen, A. 2001, [astro-ph/0110080]

Kouveliotou, C., Meegan, C. A., Fishman, G. J. et al. 1993, *ApJ*, 413, L101

Lamb, D. Q. & Reichart. 2000, *ApJ*, 536, 1

Lee, A., Bloom, E. D., & Petrosian, V. 2000a, *ApJS*, 131, 21

Lee, A., Bloom, E. D., & Petrosian, V. 2000b, *ApJS*, 131, 1

Li, H. & Fenimore, E. E. 1996, *ApJ*, 469, L115

Liang, E. & Kargatis, V. 1996, *Nature*, 381, 49

Link, B. & Epstein, R. I. 1996, *ApJ*, 466, 764

MacFadyen, A. I. & Woosley, S. E. 1999, *ApJ*, 524, 262

Mallat, S. G. & Hwang, W. L. 1992, *IEEE Transactions on Information Theory*, 38, 617

Mallat, S. G. & Zhong, S. 1992, *IEEE Transactions on Pattern Analysis and Machine Intelligence*, 7, 710

Mallozzi, R. S., Paciesas, W. S., Pendleton, G. N. et al. 1995, *ApJ*, 454, 597

Mazets, E. P., Golentskii, S. V., Ilinskii, V. N., Aptekar, R. L., & Guryan, I. A. 1979, *Nature*, 282, 587

McBreen, B., Hurley, K. J., Long, R., & Metcalfe, L. 1994, *MNRAS*, 271, 662

McBreen, S., Quilligan, F., McBreen, B., Hanlon, L., & Watson, D. 2001, *A&A Letters* (In press)

McBreen, S., McBreen, B., Quilligan, F., & Hanlon, L. 2002, *A&A Letters* (In press)

Mészáros, P. 2001, *Science*, 291, 79

Mészáros, P. & Rees, M. J. 1993, *ApJ*, 418, L59

Mészáros, P., Rees, M. J., & Wijers, R. A. M. J. 1998, *ApJ*, 499, 301

Meyer, Y. 1993, *Wavelets: Algorithms and Applications* (Philadelphia: SIAM)

Montroll, E. W. & Shlesinger, M. F. 1982, *Proc. Natl. Acad. Sci., USA.*, 79, 3380

Nakar, E. & Piran, T. 2001, [astro-ph/0103011]

Nemiroff, R. J., Norris, J. P., Wickramasinghe, W. A. D. T. et al. 1993, *ApJ*, 414, 36

Norris, J. P., Nemiroff, R. J., Bonnell, J. T. et al. 1996, *ApJ*, 459, 393

Norris, J. P., Marani, G. F., & Bonnell, J. T. 2000, *ApJ*, 534, 248

Norris, J. P., Scargle, J. D., & Bonnell, J. T. 2001, [astro-ph/0105052]

Paciesas, W. S., Meegan, C. A., Pendleton, G. N. et al. 1999, *ApJS*, 122, 465

Paczynski, B. 1991, *Acta Astron.*, 41, 257

Paczynski, B. 1998, *ApJ*, 494, L45

Panaitescu, A., Spada, M., & Mészáros, P. 1999, *ApJ*, 522, L105

Pendleton, G. N., Paciesas, W. S., Briggs, M. S. et al. 1997, *ApJ*, 489, 175

Piran, T. 1999, *Phys. Report*, 575

Preece, R. D., Briggs, M. S., Mallozzi, R. S. et al. 2000, *ApJS*, 126, 19

Quilligan, F., Hurley, K. J., McBreen, B., Hanlon, L., & Duggan, P. 1999, *A&AS*, 138, 419

Quilligan, F., McBreen, B., Hurley, K. J., Hanlon, L., Watson, D., & McBreen, S. 2000, *Proceedings of Gamma-Ray Bursts in the Afterglow Era*, Rome (In press)

Ramirez-Ruiz, E. & Fenimore, E. E. 2000, *ApJ*, 539, 712

Ramirez-Ruiz, E. & Merloni, A. 2001, *MNRAS*, 320, L25

Rees, M. J. 1999, *A&AS*, 138, 491

Rees, M. J. & Mészáros, P. 1994, *ApJ*, 430, L93

Rhoads, J. E. 1997, *ApJ*, 487, L1

Rossi, E. M., Lazzati, D., & Rees, M. J. 2001, *Proceedings of Gamma-Ray Burst and Afterglow Workshop*, Woods Hole, November 5-9 (In press)

Ruffert, M. & Janka, H.-T. 1999, *A&A*, 344, 573

Salmonson, J. D. 2000, *ApJ*, 544, L115

Sari, R. & Piran, T. 1997, *MNRAS*, 287, 110

Schaefer, B. . E., Deng, M., & Band, D. L. 2001, [astro-ph/0101461]

Schmidt, M. 2001, *ApJ*, 552, 36

Spada, M., Panaitescu, A., & Mészáros, P. 2000, *ApJ*, 537, 824

Stern, B., Poutanen, J., & Svensson, R. 1999, *ApJ*, 510, 312

Stern, B. E. & Svensson, R. 1996, *ApJ*, 469, L109

Strohmayer, T. E., Fenimore, E. E., Murakami, T. et al. 1998, *ApJ*, 500, 873

Suzuki, M., Morikawa, M., & Joichi, I. 2001, [astro-ph/0104232]

Thompson, C. 1994, *MNRAS*, 270, 480

Uman, M. 1987, *The Lightening Discharge* (London: Academic Press)

Usov, V. V. 1992, *Nature*, 357, 472

van Paradijs, J., Groot, P. J., Galama, T. et al. 1997, *Nature*, 386, 686

Young, C. A., Meredith, D. C., & Ryan, J. M. 1995, *Ap&SS*, 231, 119